NIH Public Access
Author Manuscript
*Sci Signal*. Author manuscript; available in PMC 2014 April 01.

Published in final edited form as:
*Sci Signal*. ; 6(287): ra67. doi:10.1126/scisignal.2003948.

# Interference with Akt signaling protects against myocardial infarction and death by limiting the consequences of oxidative stress

**Bethany A. Kerr**[1,†], **Lining Ma**[1,2,†], **Xiaoxia Z. West**[1], **Liang Ding**[1], **Nikolay L. Malinin**[1,‡], **Malory E. Weber**[1], **Mira Tischenko**[1], **Anna Goc**[3,4], **Payaningal R. Somanath**[3,4,5], **Marc S. Penn**[6], **Eugene A. Podrez**[1], and **Tatiana V. Byzova**[1,*]

[1]Department of Molecular Cardiology, Joseph J. Jacobs Center for Thrombosis and Vascular Biology, Lerner Research Institute, Cleveland Clinic, Cleveland, OH, 44195, USA

[2]Cardiovascular Department, Hainan Provincial People's Hospital, Hainan, China

[3]Clinical and Experimental Therapeutics, College of Pharmacy, University of Georgia, Augusta, GA, 30912

[4]Charlie Norwood VA Medical Center, Augusta, GA 30904

[5]Department of Medicine and Vascular Biology Center, Georgia Regents University, Augusta, GA 30904

[6]Integrative Medical Sciences, Northeast Ohio Medical University, Rootstown, OH, 44272

## Abstract

The intricacy of multiple feedback loops in the pathways downstream of Akt allows Akt to control multiple cellular processes in the cardiovascular system and precludes inferring consequences of its activation in specific pathological conditions. Akt1, the major Akt isoform in heart and vasculature, has a protective role in the endothelium during atherosclerosis. However, Akt1 activation has been proposed to have detrimental consequences in the cardiovascular system. Mice lacking the apolipoprotein E (ApoE), which promotes clearance of remnant lipoproteins, and the high-density lipoprotein receptor SR-BI are a model of spontaneous myocardial infarction and severe dyslipidemia. Akt1 was activated in these mice, and this activation correlated with cardiac dysfunction, hypertrophy, and fibrosis; increased infarct area; macrophage cholesterol accumulation and atherosclerosis; and reduced lifespan. Akt1 activation was associated with inflammation, oxidative stress, accumulation of oxidized lipids and increased abundance of CD36, a major sensor of oxidative stress, which created a positive feedback loop that exacerbated the consequences of oxidative stress. Thus, interference with Akt1 signaling *in vivo* could be protective and improve survival in dyslipidemia in the absence of *SR-BI* by reducing oxidative stress and responses to oxidized lipids.

[*]To whom correspondence should be addressed: Tatiana V. Byzova, Ph.D., Cleveland Clinic, NB-50, 9500 Euclid Avenue, Cleveland, OH, 44195. Telephone: 216-445-4312; Fax: 216-445-8204; byzovat@ccf.org.
[†]B.A.K. and L.M. contributed equally to this work.
[‡]Current affiliation: Department of Molecular Pharmacology and Physiology, Morsani College of Medicine, University of South Florida, Tampa, FL 33612.

Competing interests: The authors declare that they have no competing interests.

NIH-PA Author Manuscript
NIH-PA Author Manuscript
NIH-PA Author Manuscript

NIH-PA Author Manuscript

NIH-PA Author Manuscript

NIH-PA Author Manuscript

## Introduction

There is increasing interest in identifying signaling pathways that extend life span or contribute to survival in human pathologies. However, many studies focus on promoting longevity in healthy, lean models with effects similar to caloric restriction (1, 2). Conversely, the main conditions contributing to human mortality are associated with perturbed lipid metabolism and chronic inflammation resulting in atherothrombosis (thrombosis induced by atherosclerotic plaque rupture or erosion) and myocardial infarction (3, 4). The only murine model that recapitulates this process of atherothrombosis leading to death from myocardial infarction is the *ApoE*$^{-/-}$*SR-BI*$^{-/-}$ (DKO) mouse. ApoE directs triglyceride-rich lipoproteins to the liver, while SR-BI plays a key role in the reverse cholesterol transport process; thus, DKO mice have disturbed lipoprotein and cholesterol metabolism. DKO mice develop occlusive coronary arterial lesions resulting in frequent myocardial infarctions and premature death at 5–8 weeks of age (5–7). We used this model to address the role of Akt1, a kinase that regulates multiple cellular processes in the cardiovascular system, in the series of spontaneous pathological processes ending in death from myocardial infarction.

Akt1 represents 50% of the Akt activity in hearts and 70% in endothelial cells and also is the main isoform in other cells involved in atherothrombosis, including smooth muscle cells, monocytes (8) and platelets (9). Akt activation is triggered by conditions often causative for atherothrombosis, such as oxidized LDL (oxLDL) uptake (10–12). In patients, Akt is overactivated in heart failure (13, 14), after myocardial infarction (14), and in atherosclerotic plaques (11). At the cellular level, although Akt1 is a key kinase in pro-survival pathways in multiple cell types, including the endothelium (15–18), it is also involved in proinflammatory signaling in smooth muscle cells and macrophages (8). Animal models have demonstrated that although Akt1 activation is protective in some processes underlying the pathophysiology of atherothrombosis, such as endothelial dysfunction (8), it can be damaging in others, such as cardiac hypertrophy (19). In particular, Akt1 deficiency on the *ApoE*$^{-/-}$ background leads to increased endothelial damage and exacerbated atherosclerotic lesion development resulting from a Western diet (8). At the same time, in heart failure models, reduced Akt1 activation diminishes systolic dysfunction upon pressure overload (20). Intriguingly, although the Akt-dependent pathways are traditionally linked to cell survival, their inhibition has been reported to be protective in several animal models (21–23). In fact, rapamycin-mediated inhibition of mTOR (mammalian target of rapamycin), which operates both upstream and downstream of Akt, increases lifespan in various species including *C. elegans* and mice (1, 2, 15, 24). In addition, lack of Akt1 itself protects against oxidation-dependent cell senescence (25). Further, endothelial cell-specific deletion of FOXO isoforms, transcription factors that are normally degraded in response to Akt activation, is atheroprotective and causes a paradoxical reduction in Akt activation (23). Thus, due to the presence of multiple feedback mechanisms, either interference with Akt-dependent pathways or over-activation of Akt often leads to conflicting conclusions (26). Although several studies have highlighted the importance of Akt signaling in cellular processes contributing to atherothrombosis, it is unclear whether this Akt activation plays a detrimental or protective role. Moreover, extrapolation of results from these studies leads to contradictory predictions of the role of Akt1 activation in myocardial infarction associated death and underscores the importance of studying Akt signaling in different pathological settings.

We hypothesized that Akt signaling might contribute to several aspects of the pathogenesis of cardiovascular disease. Thus, we examined the role of Akt signaling in atherothrombosis and cardiac dysfunction by comparing the *ApoE*$^{-/-}$*SR-BI*$^{-/-}$(DKO) mice model of dyslipidemia and spontaneous myocardial infarction to *ApoE*$^{-/-}$*SR-BI*$^{-/-}$*Akt1*$^{-/-}$ (TKO)

NIH-PA Author Manuscript

NIH-PA Author Manuscript

NIH-PA Author Manuscript

mice. Consistent with human studies, we found that Akt activation is substantially increased under conditions of dyslipidemia caused by lack of *ApoE* and *SR-BI*. We then show that Akt1 activation contributes to myocardial infarction and mortality in this model. Akt1 activation was associated with reactive oxygen species (ROS) production, accumulation of oxidized lipids and their recognition by increasing the abundance of the scavenger receptor CD36, the major receptor for oxidized phospholipids that is involved in proinflammatory signaling and macrophage foam cell formation. Blockade or deletion of CD36 on DKO macrophages led to reduced foam cell formation to the amount observed in TKO mice. Thus, under conditions of severe dyslipidemia in the absence of *SR-BI*, Akt signaling contributes to atherothrombosis and promotes mortality from myocardial infarction.

## Results

### Akt1 activation is increased in DKO mice with dyslipidemia and spontaneous myocardial infarction

To assess the consequences of Akt signaling, we utilized $ApoE^{-/-}SR\text{-}BI^{-/-}$ (DKO) mice which develop dyslipidemia, spontaneous atherosclerosis and heart disease (5–7). In agreement with human studies (13, 14), phosphorylation of Akt at $Ser^{473}$ in hearts of DKO mice was increased by 2.5-fold compared to wild-type mice (Fig. 1A). At the same time, phosphorylation of Akt at $Thr^{308}$ in DKO hearts was also higher. Pan-Akt immunoblotting demonstrated that the total abundance of Akt was decreased in $ApoE^{-/-}SR\text{-}BI^{-/-}Akt1^{-/-}$ (TKO) mice compared with DKO mice. As a result of Akt1 deletion in TKO mice, the phosphorylation of Akt was reduced by 2.6-fold at $Ser^{473}$ and 5.6-fold at $Thr^{308}$ compared to DKO mice, reaching a value of 67% of the phosphorylation of Akt at $Ser^{473}$ in wild-type mice (Fig. 1A). Although the abundance of Akt2, but not that of Akt3, was increased in hearts after Akt1 deletion (Fig. S1A), there was no compensation in Akt phosphorylation since $Ser^{473}$ phosphorylation was not increased in TKO compared to wild-type (Fig.1A). Consequently, Akt activity, as determined by the phosphorylation of the downstream target glycogen synthase kinase (GSK)-3, was also reduced 4.2-fold in TKO mice compared to DKO mice (Fig. 1A). Total GSK-3 did not appear to be substantially different between groups. Correspondingly, phosphorylation of Akt at both $Thr^{308}$ and $Ser^{473}$ appeared higher in the aorta and livers of DKO mice than in those of wild-type mice, although the change was insignificant (Fig. S1B). Similarly, phosphorylation of GSK-3 was higher in the aortas of DKO mice compared with those of TKO mice, but the increase was insignificant in the livers (Fig. S1B). Kinase assays indicated that Akt activity was higher in DKO hearts and macrophages compared with wild-type and TKO mice (Fig. S1C).

### Akt1 deficiency improves the survival of DKO mice

The severe dyslipidemia, atherosclerosis, and spontaneous myocardial infarctions in DKO mice results in shortened lifespan, with most of the mice dying between 5 and 8 weeks of age (5, 6). To assess the effect of Akt1 ablation on longevity, we examined the lifespan of DKO and TKO mice (Fig. 1B,C). Indeed, survival of TKO mice was improved compared to DKO mice, especially at later stages (from 50 to 60 days of age) (Fig. 1C). Substantial differences in survival between DKO and TKO mice were observed from day 45 (Fig. 1B), with DKO mice dying at a faster rate (hazard ratio=4.19). The median survival time (45 days for DKO, 50 days for TKO) was also significantly increased upon Akt1 deletion (Fig. 1C), resulting in an increased survival of 11% in TKO mice compared with DKO mice, which is similar to the increase seen with rapamycin treatment (1). Thus Akt1 deletion promotes longevity in the DKO mouse, a finding that is consistent with previous studies of Akt1 interference in various organisms and diseases (15, 16, 24). Deletion of Akt1 was associated not only with prolonged lifespan in this model, but also with improved reproductive characteristics of DKO breeder mice (Table S1). The breeders of both genotypes were

NIH-PA Author Manuscript

NIH-PA Author Manuscript

NIH-PA Author Manuscript

heterozygous for *SR-BI* and the frequency of KO births was below the expected ratio. The KO frequency was higher for DKO breeders, indicating no change in embryonic death in DKO mice compared with TKO mice. In contrast, there were more litters per female and pups per litter for TKO breeders compared with DKO breeders (Table S1). In addition to improved survival, TKO breeders were fertile for almost 4 months longer than DKO breeders (Table S1) and Akt1 deletion also resulted in diminished body size of the mice (Fig. S2), as previously reported (27). These data demonstrate that Akt1 deletion is associated with improved survival of mice on the DKO background.

### Akt1 deficiency improves cardiac function and diminishes cardiac hypertrophy

Because Akt activation is increased in humans and mice with atherosclerosis and cardiac dysfunction, we hypothesized that deletion of at least one Akt isoform, Akt1, might alleviate the severe cardiac dysfunction leading to premature death observed in DKO mice (6). Indeed, based on results of echocardiography (Fig. 1D), TKO mice displayed improved cardiac function compared with DKO mice, although cardiac function was not returned to wild-type values. We analyzed left ventricular function in mice between 4 and 7 weeks of age, the time during which the most adverse cardiac events occur in DKO mice. Using echocardiography we calculated the ejection fraction which measures the volumetric fraction of blood pumped out of the left ventricle and which decreases with deleterious cardiac remodeling. Reductions in the ejection fraction due to loss in contraction accounts for cardiac dysfunction. Fraction of shortening was used as a measure of ventricular function and quantifies the changes in ventricular luminal dimensions in diastole and systole. Ventricular dimensions increase with mechanical demand and thus increased fraction of shortening represents ventricles which are not able to efficiently contract resulting in cardiac dysfunction. Until 6 weeks of age, the ejection fraction and fraction of shortening were not significantly different between TKO and DKO mice (Fig. 1E,F). However, during the $7^{th}$ week of age, when peak mortality occurred (Fig. 1B), TKO mice had significantly increased ejection fraction and fraction of shortening compared with DKO mice (Fig. 1E,F). Thus, Akt1 deletion led to delayed development of cardiac dysfunction. Correspondingly, in a coronary ligation model, Akt1 deletion resulted in reduced damage by myocardial infarction (Fig. S3), although this does not indicate a direct protective effect on cardiomyocytes due to possible changes in remodeling, infiltration and inflammation. Thus, inhibition of Akt activation appears to be cardioprotective. The main consequence of cardiac dysfunction is hypertrophy of the heart. DKO mice exhibited a significantly increased (1.8-fold) heart weight to body weight ratio compared with wild-type mice (Fig. 1G,H). The heart weight to body weight ratio of TKO mice was higher than wild-type mice, but was significantly decreased (1.2-fold) compared with DKO mice (Fig. 1G,H). Thus, in this model of spontaneous cardiac dysfunction, activation of Akt1 signaling contributes to cardiac hypertrophy.

### Cardiac fibrosis and necrosis are diminished in TKO mice

Because Akt1 deletion improved cardiac function in DKO mice, we next determined size of myocardial infarction lesions. Sites of myocardial infarctions were visible on both DKO and TKO hearts (Fig. 1G, arrows); however, the infarctions on TKO hearts appeared smaller. To quantify lesions, heart sections were stained with Masson's trichrome to differentiate healthy heart tissue (red) from fibrotic tissue (blue) (Fig. 2A). The percentage of fibrotic area in TKO hearts was 20.1-fold lower than in DKO hearts (Fig. 2B). In addition, H&E staining of serial tissue sections (Fig. 2C) revealed that necrotic area in TKO hearts was decreased 5.8-fold compared with DKO hearts (Fig. 2D). Thus, Akt1 deletion was associated with decreased development of cardiac pathologies associated with cardiac dysfunction. This is consistent with previous reports demonstrating that increased Akt activation promotes fibrosis especially in the heart (28, 29).

NIH-PA Author Manuscript

NIH-PA Author Manuscript

NIH-PA Author Manuscript

Myocardial apoptosis plays a critical role in heart failure and ischemic heart disease. We used TUNEL staining to visualize cardiomyocyte apoptosis (Fig. 2E) and found that apoptosis was diminished 1.5-fold in TKO hearts compared with DKO hearts (Fig. 2F). However, both DKO (4.1-fold) and TKO (2.6-fold) hearts exhibited higher rates of apoptosis compared with wild-type hearts (Fig. 2F).

## Atherosclerotic lesions progression but not blood cholesterol amounts are diminished in TKO mice

To determine if improved cardiac function in TKO mice was due to reduced atherosclerosis, we quantified lipid accumulation in the aortic root. Oil red O staining of aortic root sections indicated that lesions were 2.5-fold smaller in TKO mice than those in DKO mice (Fig. 3A,B). Analysis of entire aortas (Fig. 3C) revealed that the percentage of aortic area containing plaques was decreased 2.7-fold in TKO mice compared with DKO mice (Fig. 3D). Likewise, lipid accumulation by macrophages resulting in the formation of foam cells *in vitro* was 1.6-fold higher in DKO macrophages compared with TKO macrophages (Fig. 4A,B). Akt1 deletion on the *ApoE* background alone did not result in changes in aortic plaque area but did lead to significantly decreased foam cell formation (Fig. S4A–D). DKO mice had large atherosclerotic coronary lesions, whereas TKO mice had a 17.0-fold decrease in the number of lesions per heart (Fig. 4C,D). $ApoE^{-/-}$ and $ApoE^{-/-}Akt1^{-/-}$ mice also displayed an average of less than one coronary lesion per heart (Fig. S4E). $ApoE^{-/-}$ mice have similar Akt activity as wild-type mice when fed chow diet and show a small, but insignificant increase in Akt activity only after being placed on a Western diet (Fig. S1C). Thus, these results suggest that Akt1 activity is substantially increased only in mice experiencing hyperlipidemic conditions, such as a Western-style diet or because of combined *ApoE* and *SR-BI* deletion. These data suggest that lack of Akt1 in DKO mice retards the progression of atherosclerosis.

Another characteristic feature of DKO mice is altered liver function and hypertrophy. As with hearts, DKO mice displayed larger livers compared with wild-type and TKO mice (Fig. S5A). The liver weight to body weight ratio for DKO mice was significantly higher than both wild-type and TKO mice (Fig. S5B).

Because Akt1 deficiency reduced atherosclerotic plaque formation, we used *en face* staining of aortas to assess the abundance of VCAM-1, which predisposes aortic endothelium to atherosclerosis (30–32). Endothelial cells were visualized using CD31 staining (Fig. 4E). As anticipated, VCAM-1 staining was increased in atherosclerotic DKO aortas by 7.7-fold compared with wild-type aortas (Fig. 4F). VCAM-1 abundance was diminished 2.8-fold in TKO mice compared with DKO mice (Fig. 4F). Therefore, Akt deficiency is associated with decreased VCAM-1 abundance, suggesting a reduction in proinflammatory processes and susceptibility to atherosclerosis.

To determine the effects of Akt1 deletion on the proinflammatory signature of endothelial cells, we examined atherosclerotic gene expression in isolated endothelial cells (Table S2). Akt1 deletion resulted in the increased expression of several genes encoding growth factors, such as platelet derived growth factor, osteopontin, vascular endothelial growth factor, and transforming growth factor β2. In addition, several pro-apoptotic and inflammatory genes showed decreased expression in TKO endothelial cells compared with DKO endothelial cells (Table S2). Thus, deletion of Akt1 in a model of dyslipidemia and cardiac dysfunction results in a pro-survival gene expression pattern.

Multiple pathological aspects of cardiac problems in DKO mice, as described above, are caused by severe dyslipidemia in the absence of *SR-BI*. Therefore, we addressed whether Akt1 deletion alters lipid production and cholesterol concentrations in DKO mice.

NIH-PA Author Manuscript

NIH-PA Author Manuscript

NIH-PA Author Manuscript

Surprisingly, cholesterol concentrations in the blood were similar between DKO and TKO mice (Fig. S5C). DKO mice produce abnormal high-density lipoprotein particles which are found in the very low-density lipoprotein, intermediate-density lipoprotein, and low-density lipoprotein fractions, a phenomenon that was also seen in the blood of TKO mice (Fig. S5D). Thus, the protective effect of Akt1 deletion is not mediated by changes in the cholesterol concentration.

## Reactive oxygen species generation and lipid oxidation are diminished in the absence of Akt1

Oxidative stress in general and the presence of oxidized lipids promote atherogenesis and Akt activation promotes both ROS production and its degradation (25). The plasma concentration of hydrogen peroxide ($H_2O_2$) was more than 2.0-fold higher in DKO mice compared to wild-type mice and Akt1 deficiency in TKO mice produced a 1.6-fold decrease in $H_2O_2$, resulting in concentrations similar to those in wild-type mice (Fig. 5A). In addition, dihydroethidium staining of heart tissue sections indicated that superoxide anion production was also increased in DKO mice compared to wild-type mice and that the lack of Akt1 in TKO mice was associated with ROS production similar to that in wild-type mice (Fig. 5B,C). At the same time, there were no differences between wild-type, DKO, and TKO mice in the plasma concentrations of the antioxidants superoxide dismutase and catalase (Fig. S6A,B). In addition, the plasma concentrations of peroxynitrite did not differ significantly between wild-type, DKO, and TKO mice (Fig. S6C) suggesting that nitric oxide acting as a scavenger of the superoxide anion did not contribute substantially to the observed phenotype (33). Thus, Akt1 deficiency may reduce the amount of ROS by decreasing their generation.

To assess the consequences of increased oxidative stress, we stained heart tissues for end products of polyunsaturated fatty acid oxidation (34): CEP (ω-(2–carboxyethyl pyrrole)) (Fig. 5D) and CPP (2–(ω-carboxypropyl) pyrrole) (Fig. S6D). Lipid oxidation in heart tissues appeared to result from the DKO genotype because little CEP or CPP was detected in wild-type hearts (Fig. 5D,E and S6D,E). Consistent with the ROS measurements, the amount of lipid oxidation as judged by CEP abundance was 4.3-fold lower in TKO hearts compared with DKO hearts (Fig. 5E). CPP abundance demonstrated similar tendencies, although the differences between DKO and TKO hearts were not statistically significant (Fig. S6E). We have previously demonstrated that inflammation and oxidative stress promotes the accumulation of these pyrroles in various tissues (34). Indeed, staining for the neutrophil marker Gr-1 (lymphocyte antigen 6C/G) in wild-type, DKO, and TKO hearts overlapped with CEP staining (Fig. 5D,E). Likewise, co-staining with the macrophage marker CD68 revealed increased macrophage infiltration into damaged heart tissue in DKO mice (87–fold) compared with wild-type mice (Fig. 5E). TKO hearts contained 1.6-fold fewer macrophages and 11.9-fold fewer neutrophils compared with DKO hearts (Fig. 5E). This decrease in inflammatory cell recruitment and oxidative stress upon Akt1 deletion may account for the reduction in atherogenesis and consequent myocardial damage in TKO hearts. Corresponding to the increased oxidative stress in DKO hearts, plasma concentrations of CEP were 1.9-fold increased in DKO mice compared with TKO mice (Fig. 5F).

A key prerequisite of the inflammatory response is activation of the NF-κB pathway (35), which, in turn, is directly affected by Akt signaling (36). We stained hearts for phosphorylated IKKα/β, which stimulates NF-κB activity (Fig. 5G). Indeed, the amount of phosphorylated IKKα/β was ~8-fold higher in DKO mice compared to wild-type mice (Fig. 5G), which is consistent with the high amount of inflammation in these mice (Fig.5D). The lack of Akt1 resulted in 1.9-fold decrease in phosphorylated IKKα/β in the hearts of TKO mice compared with DKO mice (Fig. 5H). Thus, Akt1 deletion is associated with attenuated

NIH-PA Author Manuscript

NIH-PA Author Manuscript

NIH-PA Author Manuscript

NF-κB activation in hearts of DKO mice providing a possible mechanism for Akt1's effects on inflammation and ROS accumulation.

### Akt1 decreases ROS generation in endothelial cells and macrophages

To determine the contribution of various cell types in the phenotype of TKO mice, we measured the ROS production by isolated endothelial cells. The basal concentration of ROS production by unstimulated cells was highest in DKO endothelial cells compared with wild-type (1.5-fold) and TKO (1.3-fold) endothelial cells (Fig. 6A). When treated with oxLDL to mimic dyslipidemia, ROS production was increased over basal for all groups, although DKO endothelial cells were the highest producers of ROS (Fig. 6A). A similar trend was observed in isolated macrophages. Under basal conditions, wild-type and DKO macrophages produced similar amounts of ROS, whereas TKO macrophages produced 1.3-fold and 1.5-fold less ROS (Fig. 6B). Treatment of DKO macrophages with oxLDL triggered a small, but significant, increase in ROS (Fig. 6B).

Likewise, Akt1 deletion led to decreased formation of reactive nitrogen species produced by DKO endothelial cells. Consistent with our previous results, nitrotyrosine concentration was increased in DKO endothelial cells 5.5-fold over wild-type cells (Fig. 6C). TKO endothelial cells contained 3.3-fold less nitrotyrosine than DKO cells (Fig. 6C). Thus, Akt1 deletion was associated with reductions in the reactive oxygen and nitrogen species generated by endothelial cells and macrophages.

### Akt1 deficiency correlates with improved survival after oxidation challenge in endothelial cells and macrophages

Because Akt has been reported to promote not only ROS generation but also sensitivity to oxidative stress (25), we assessed survival of cells exposed to oxidized LDL, a main factor that promotes atherogenesis. Under these conditions, the rate of cell death was more than 50% higher in DKO cells than in TKO or wild-type endothelial cells (Fig. 6D). For oxLDL-treated macrophages, the rate of cell death for DKO cells was 2.7-fold higher than in wild-type or TKO macrophages (Fig. 6E). Thus, DKO macrophages and endothelial cells were susceptible to cell death in the presence of oxLDL and deletion of Akt1 is associated with rescue of these cells to the survival percentages observed in wild-type cells.

### Akt1 activity is associated with increased CD36 abundance, which contributes to foam cell formation

In *ApoE*$^{-/-}$*SR-BI*$^{-/-}$ DKO cells, the main scavenger receptor responsible for the recognition and sequestration of oxLDL is CD36 (37). This suggests that the lack of Akt1 might lead to reduced abundance of the proatherogenic receptor CD36, which, in turn, might account for the overall reduced atherogenesis and sensitivity to oxidative stress in TKO mice. Indeed, CD36 protein abundance in hearts of DKO mice was 2.4-fold higher than wild-type hearts and the lack of Akt1 was associated with a reduction in CD36 abundance in TKO hearts to an amount similar to that in wild-type hearts (Fig. 7A,B). This effect of Akt1 deletion on CD36 was more prominent for macrophages than for endothelial cells. FACS analysis indicated that CD36 cell surface abundance was 1.9-fold higher on DKO macrophages compared with wild-type macrophages and that the surface abundance of CD36 was similar in TKO and wild-type macrophages (Fig. 7C). In endothelial cells, the difference between DKO and TKO cell CD36 surface abundance was not statistically significant (Fig. 7D). The increased in CD36 protein abundance in DKO macrophages was confirmed by immunoblotting (Fig. S7). Deletion of Akt1 on the *ApoE* background had no effect on CD36 abundance on macrophages (Fig. S8), likely due to the absence of dyslipidemia which occurs only upon *SR-BI* deletion.

NIH-PA Author Manuscript

NIH-PA Author Manuscript

NIH-PA Author Manuscript

Together, the results suggested that Akt1 controls atherogenesis and foam cell formation both *in vitro* and *in vivo* by regulation of CD36 surface abundance on macrophages. Therefore, we assessed whether the blockade of CD36 on DKO macrophages might diminish foam cell formation to numbers similar to wild-type or TKO macrophages (Fig. 7E). Macrophages from DKO mice generated 1.8-fold more foam cells compared with wild-type macrophages (Fig. 7F). Treatment with a previously characterized CD36 blocking peptide (38) diminished foam cell generation by DKO macrophages in a concentration-dependent manner (Fig. 7F). Thus, the numbers of foam cells generated from DKO macrophages upon CD36 blockade were similar to those generated by TKO macrophages or wild-type macrophages and 1.5-fold higher without treatment (Fig. 7F). Treatment with CD36 blocking peptides also diminished wild-type and TKO foam cell formation because CD36 is also present on these macrophages (Fig. S9). To confirm the importance of CD36 in DKO foam cell formation and coronary atherosclerosis, we generated *SR-BI*$^{-/-}$*ApoE*$^{-/-}$*CD36*$^{-/-}$ mice. Plasma concentrations of CEP were significantly higher in *SR-BI*$^{-/-}$*ApoE*$^{-/-}$*CD36*$^{-/-}$ compared with TKO and wild-type mice (Fig. 8A), indicating that systemic oxidative stress is not mediated by CD36 in DKO mice. In contrast, macrophages isolated from these *SR-BI*$^{-/-}$*ApoE*$^{-/-}$*CD36*$^{-/-}$ mice generated foam cells when exposed to oxLDL at rates similar to wild-type and TKO macrophages (Fig. 8B,C), suggesting that the Akt1-CD36 cross-talk is required for foam cell formation in DKO mice. In addition, coronary artery plaque formation was similar in *SR-BI*$^{-/-}$*ApoE*$^{-/-}$*CD36*$^{-/-}$ and TKO mice, whereas wild-type mice had no identifiable lesions (Fig. 8D,E). These data suggest that increased CD36 abundance in DKO mice may be responsible for the enhanced foam cell formation and coronary atherosclerosis, but does not affect the oxidative stress accumulation in tissues. Thus, conditions of dyslipidemia and oxidative stress led to increased CD36 abundance and foam cell formation in DKO mice and deletion of Akt1 provided protection, potentially by decreasing the surface abundance of CD36 on macrophages.

## Discussion

Although several studies have demonstrated increased activation of the Akt pathway in hyperlipidemia and heart failure in humans (13, 14), it remained unclear whether this phenomenon promotes heart disease and atherothrombosis or contributes to a protective response. Further, it appears that not only activation of Akt, but also the duration of its activation is of key importance with short-term Akt activation being beneficial for cardiac tissue and prolonged activation of Akt being detrimental (26, 39). In this study, we utilized the *ApoE*$^{-/-}$*SR-BI*$^{-/-}$ DKO mouse, which models the severe cardiac dysfunction of human coronary heart disease resulting in spontaneous myocardial infarction and premature death (6), to examine the role of Akt1 in atherothrombosis. Global deletion of Akt1 on the DKO background led to diminished Akt activity and resulted in substantial alleviation of many pathological features of heart disease in DKO mice. Lack of Akt1 was associated with improved survival in DKO mice, especially at the later stage of the disease when mice experience myocardial infarctions. Multiple complications leading to death in this model, such as cardiac dysfunction, hypertrophy, and cardiac fibrosis, were substantially reduced. These changes may reflect reduced inflammation, foam cell formation and diminished atherosclerotic lesions in TKO mice *in vivo*. ROS production is a main systemic contributing factor to atherosclerosis especially under conditions of dyslipidemia and was reduced in hearts, plasma, endothelial cells, and macrophages after Akt1 deletion. Lack of Akt1 correlated with decreased surface abundance of CD36, a key oxidized lipid receptor that contributes to atherogenesis in hearts, on endothelial cells, and on macrophages. Thus, during dyslipidemia and cardiac dysfunction, chronic Akt1 activation is associated with increased oxidative stress and proatherogenic lipid oxidation product generation and their

NIH-PA Author Manuscript

NIH-PA Author Manuscript

NIH-PA Author Manuscript

recognition, resulting in enhanced atherosclerosis and spontaneous myocardial infarction and global deletion of Akt1 substantially diminishes these responses.

Our results suggest that excessive Akt1 activation is detrimental under the conditions of dyslipidemia and inflammation endemic in the DKO mouse, which is seemingly different to the protective role of Akt1 in *ApoE*$^{-/-}$ single KO mice (8). In contrast to the *ApoE*$^{-/-}$ mice, DKO mice show diet-independent changes in lipid profiles with high cholesterol concentrations in the blood due to blocked cholesterol accumulation by liver, leading to accelerated detrimental changes in the vessel wall, lipid accumulation and many of the attributes of not only atherosclerosis but the complete atherothrombosis process. We show that lipid abnormalities in DKO mice were accompanied by high oxidative stress concentrations, which exacerbated pathological changes. In our TKO mouse model we did not observe a reduction in endothelial cell survival due to lack of Akt1, which is similar to the FOXO triple knockout model (23). The SR-BI receptor mediates the main protective signaling pathway for endothelium, especially in hyperlipidemia, which involves activation of Akt-eNOS pathway (8, 40), which can inhibit the activation of NF-κB signaling induced by VCAM-1 on endothelial cells (32, 41). Indeed, lack of Akt1 on the *ApoE*$^{-/-}$ background disrupts this protective eNOS-regulated mechanism, leading to increased endothelial apoptosis, which, in turn, results in exacerbated atherosclerosis in *ApoE*$^{-/-}$*Akt1*$^{-/-}$ mice (8). Despite reduced oxLDL sequestration and foam cell formation from macrophages upon Akt1 deletion, endothelial damage is a predominant feature in this *ApoE*$^{-/-}$*Akt1*$^{-/-}$ mouse model that largely accounts for the overall phenotype (8). In *ApoE*$^{-/-}$*SR-BI*$^{-/-}$ DKO mice, however, this Akt-eNOS dependent atheroprotective signaling on the endothelium is not operational due to the lack of SR-BI receptor. Deletion of Akt1 in *ApoE*$^{-/-}$*SR-BI*$^{-/-}$ DKO mice resulted in anti-inflammatory effects on the endothelium due to reduced NF-κB signaling as has been previously reported in another model (42) and evidenced by decreased expression of genes encoding proinflammatory factors in endothelial cells in TKO mice compared with DKO mice. Instead, Akt deficiency on the DKO background was associated with reduced ROS generation and systemic oxidative stress and diminished lipid oxidation, binding, and accumulation due to low CD36 surface abundance on macrophages. In addition, Akt1-null mice display mild deficiencies in platelet activation (43, 44), which might influence the final events of atherothrombosis in DKO mice, which die from thrombotic events. However, the subtle nature of the platelet phenotype in Akt1-null mice makes it unlikely that decreased platelet aggregation plays a leading role in TKO mice, which survived longer but eventually died from causes similar to those of their DKO counterparts. Further, although the *ApoE*$^{-/-}$ mouse primarily models only the process of atherogenesis, the DKO mouse has a cardiac phenotype characterized by heart enlargement, fibrosis, cardiac dysfunction, and myocardial infarction leading to shortened lifespan (6, 7). Previous studies have linked Akt activity to hypertrophy, in which overexpression of Akt1 stimulates cardiac hypertrophy (45), and inactivation of Akt1 diminishes cardiac hypertrophy resulting in heart weight to body weight ratios similar to controls (46). Corroborating our data that Akt1 over-activation in DKO mice resulted in diminished survival, cardiac-specific Akt1 overexpression results in early mortality, likely due to heart failure. Hearts from these mice are hypertrophic and fibrotic, and show cardiac dysfunction (46). Correspondingly, Akt1 inactivation in DKO mice was associated with reduced hypertrophy, fibrosis and necrosis, and improved cardiac function. Together, the combined pathological conditions in DKO mice resultrd in increased activation of Akt in heart, which is reminiscent of related human pathologies.

The main feature of TKO mice that appeared to account for the overall phenotype was reduced oxidative stress and its consequences, such as lipid oxidation and accumulation in foam cells, although the concentrations of cholesterol and lipids in DKO and TKO mice were similar. Indeed, previous studies show that Akt1 signaling promotes oxygen

NIH-PA Author Manuscript

NIH-PA Author Manuscript

NIH-PA Author Manuscript

consumption and ROS production, thereby providing a mechanism for the reduced senescence in Akt1 null mice (25). Other studies show that Akt signaling elevates ROS concentrations by multiple mechanisms, including inhibition of intracellular and extracellular ROS scavenging (25, 47–51). Thus, multiple pathways leading to ROS accumulation might be affected by global Akt1 deletion. Knockout of three *FOXO* genes in endothelial cells results in decreased Akt activity and an anti-atherogenic phenotype (23), consistent with the results of our Akt1 deletion model.

Combined deletion of ApoE and SR-BI resulted in enhanced CD36 abundance, an effect that was reversed by Akt1 deletion. In the absence of SR-BI, CD36 is the main scavenger receptor that binds to and sequesters oxLDL to promote foam cell formation (52). We demonstrated that there was a correlation between Akt1 activation and CD36 abundance under conditions of dyslipidemia and oxidative stress. CD36 is required for oxLDL uptake, foam cell formation, macrophage survival after oxLDL treatment and macrophage recruitment into inflamed tissues. CD36 deficient $ApoE^{-/-}$ macrophages accumulate less oxLDL resulting in diminished foam cell formation *in vitro* and *in vivo* (52) which has been confirmed in human macrophages deficient in CD36 (53). Accordingly, because of reduced CD36 abundance, TKO macrophages accumulate less oxLDL. This is consistent with the results of multiple studies that implicate Akt signaling in oxLDL uptake (11, 54–56). We showed that blockade or deletion of CD36 in DKO mice resulted in diminished foam cell formation and mimicked the phenotype caused by inactivation of Akt1. Thus, Akt1-dependent regulation of CD36 may be the main mechanism responsible for increased foam cell formation and atherogenesis in DKO mice. Thus, in DKO mice which show dyslipidemia, oxidation and cardiac dysfunction, increased Akt1 activation stimulated both ROS-mediated lipid oxidation and their recognition by CD36, resulting in enhanced oxLDL generation, accumulation and foam cell formation. Together, this creates a vicious cycle of oxidative imbalance promoting further tissue damage and even more ROS production (57) thereby resulting in atherothrombosis and death. Although the use of systemic inhibitors of all Akt isoforms in metabolic pathologies seems unlikely due to a number of possible complications (58), in this model, lack of the Akt1 isoform was associated with improved survival and alleviation of multiple complications of heart disease and spontaneous myocardial infarction caused by ApoE and SR-BI deletion. Our findings reveal that CD36 abundance and signaling in combination with Akt1 activation promotes atherothrombosis and this signaling axis needs to be further explored. Thus, targeted stabilization or prevention the increase in Akt activation during atherogenesis might be beneficial for the treatment of atherothrombosis and its complications.

## Materials and Methods

### Animals

C57BL/6, $ApoE^{-/-}$ (C57BL/6 background), and $SR\text{-}BI^{+/-}ApoE^{-/-}$ (mixed C57BL/6×S129 background) mice were purchased from Jackson Laboratories. $SR\text{-}BI^{+/-}ApoE^{-/-}$ mice were backcrossed to C57BL/6 background for 10 generations. $Akt1^{-/-}$ mice were generated as previously described (9) and backcrossed to the C57BL/6 background for 10 generations. $SR\text{-}BI^{-/-}ApoE^{-/-}$ (DKO) mice were generated by intercrossing $SR\text{-}BI^{+/-}ApoE^{-/-}$ mice. $SR\text{-}BI^{-/-}ApoE^{-/-}Akt1^{-/-}$ (TKO) mice were generated by first crossing $Akt1^{-/-}$ mice with $SR\text{-}BI^{+/-}ApoE^{-/-}$ mice. The offspring $SR\text{-}BI^{+/-}ApoE^{+/-}Akt1^{+/-}$ females were then crossed with sibling $SR\text{-}BI^{+/-}ApoE^{+/-}Akt1^{+/-}$ to generate $SR\text{-}BI^{+/-}ApoE^{-/-}Akt1^{-/-}$ which were intercrossed with siblings to generate TKO mice. DKO and TKO breeder mice were heterozygous for *SR-BI* because the *SR-BI* knockout results in infertility (7). $SR\text{-}BI^{-/-}ApoE^{-/-}CD36^{-/-}$ (on a C57BL/6 background) were generated using a similar breeding scheme. Animals were fed a standard chow diet. Mice were sacrificed at 42 days of

NIH-PA Author Manuscript

NIH-PA Author Manuscript

NIH-PA Author Manuscript

age for most experiments. All animal procedures were performed in accordance the Institutional Animal Care and Use Committee of the Cleveland Clinic guidelines.

### Immunoblotting

Hearts were homogenized in RIPA buffer (Cell Signaling). 40μg of protein per sample was separated by electrophoreses and transferred to a PVDF membrane. Proteins were detected with anti-Akt1, anti-phospho-Akt, anti-phospho-GSK-3α/β or anti-GSK-3β (Cell Signaling) antibodies. Murine lung endothelial cells (MLECs) or macrophages were treated with 12μg/mL oxLDL for 10 min and then lysed in buffer containing 1% Triton, 150mM NaCl, 50mM Tris pH7.4 and protease inhibitor cocktail. Whole cell lysates were separated, transferred to PVDF membrane, and analyzed by immunoblotting using the anti-CD36 antibody (Cayman Chemicals) and the anti-GAPDH antibody (Santa Cruz Biotechnology) as a loading control.

### Echocardiography

Cardiac function was evaluated weekly using a 14MHz linear array transducer interfaced with a Sequoia C256 (Acuson) when mice were between 4 and 7 weeks of age. Once clear views of the long axis and the short axis were achieved, M mode analysis was performed to measure ejection fraction (EF) and fraction of shortening (FS), which were calculated using the Vevo cardiac measurements software package. FS is calculated as percent change in the loss of contraction (ED-ES/ED × 100%), where ED is the ventricular luminal dimension in diastole and ES is the dimension in systole.

### Cardiac fibrosis and necrosis quantification

Mice were sacrificed at 6 weeks of age when cardiac dysfunction was just becoming apparent to assess the role of Akt1 deletion in cardiac pathogenesis. Mice were euthanized and perfused through the left ventricle with PBS. Hearts were immersion-fixed in buffered 10% formalin. Hearts were cut at the mid level transversely, as described previously (19, 59), and embedded in paraffin. Serial sections (8μm) were cut and stained with H&E or Masson's trichrome. To quantify fibrosis, five images were taken of four sections per Masson's trichrome stained heart on an Olympus BX51 microscope. Cardiac fibrosis was quantified by measuring the total stained area the total area of the heart using the Image Pro software. To quantify necrosis, five images were taken of four sections per H&E stained heart on an Olympus BX51 microscope. The necrotic area was measured and normalized to the total area of the heart using the Image Pro software.

### Atherosclerotic Lesion Measurements

Atherosclerotic lesions were quantified by *en face* aortic coverage measured by computer-assisted planimetry and analysis of lesion area at the aortic root was performed as previously described (60). Briefly, the hearts were perfused with PBS and then 4% paraformaldehyde (PFA) overnight. The entire aortic tree, including the heart, was dissected free of fat and other tissue. Aortae were cut open longitudinally, stained with Oil red O, and digitally scanned. Lesion area was assessed using Adobe Photoshop software. Hearts were infiltrated with 30% sucrose, frozen in OCT, and cut into serial cryosections of 10μm thickness. Sections were cut from the region of the proximal aorta through the aortic sinuses and stained with Oil red O and fast green. Morphometric evaluations of lesion size were made using Image-Pro software.

### Peritoneal Macrophage Isolation

Peritoneal macrophages were elicited from mice 3 days after intraperitoneal injection of 3% Brewer thioglycollate medium. Macrophages were harvested by lavage, centrifuged, and cultured in RPMI1640 medium containing 10% FBS, 100U/mL penicillin, and 100μg/mL

NIH-PA Author Manuscript

NIH-PA Author Manuscript

NIH-PA Author Manuscript

streptomycin for 2 hr. Non adherent cells were removed by gentle washing with RPMI1640 medium. Adherent cells were maintained in culture until used for experiments.

### Foam Cell Formation

Macrophages were cultured in 25μg/mL oxidized LDL (oxLDL; generated as previously described (61)) and 2μM CD36 or scrambled peptides (which were previously described (38)) for 24 hr. Cells were fixed and stained with hematoxylin and Oil Red O according to standard protocols. Images were acquired (Leica TCS-SP) and quantification of Oil Red O positive cells was performed using the Image Pro Plus software.

### En Face Immunostaining

VCAM-1 expression (Santa Cruz) was assessed in endothelial cells, as demonstrated by CD31 (Abbiotec) staining, in the aortic arch and descending thoracic aorta by *en face* staining, followed by laser-scanning confocal microscopy (Leica TCS-SP) as previously described (62).

### In situ TUNEL Staining

Hearts were embedded in optimal cutting temperature (OCT) freezing medium and sectioned at 7μm. Sections were then fixed in 4% PFA and analyzed for TUNEL staining using the *In Situ* Cell Death Detection Kit, TMR Red (Roche) according to the manufacturer's protocol. Slides were mounted and imaged using a Nikon ZMZ1000 fluorescent microscope. The fluorescence intensity was quantitatively determined using MetaMorph software.

### In situ detection of superoxide

Dihydroethidium (DHE, Invitrogen) staining for superoxide was carried out as previously described (63). Briefly, hearts were harvested, embedded in OCT, and cryosectioned at 8μm. DHE (10μM) was applied to each tissue section and slides were incubated for 30 min at 37°C. Slides were imaged using a fluorescence microscope (Nikon ZMZ1000). The fluorescence intensity was quantitatively determined using MetaMorph software.

### Immunofluorescent Staining

Hearts were embedded in OCT freezing medium and sectioned at 7μm. Sections were then fixed in 4% PFA and incubated with primary antibodies: rabbit anti-CEP (64), rat anti-CD68 (AbD Serotec), rat anti-Ly-6G/Gr-1 (BD Pharmigen), and rabbit anti-phospho IKKα/β (Cell Signaling). Tissues were then washed in PBS and exposed to a fluorescently labeled secondary antibody: goat anti-rabbit Alexa Fluor488, anti-rabbit Alexa Flour568, or anti-rat Alexa Fluor568 (Invitrogen). Slides were mounted and images were taken using either a TCS-SP (Leica) or a ZMZ1000 (Nikon) microscope. The images were quantified using ImagePro software (Media Cybernetics).

### Murine Lung Endothelial Cell Isolation

Lungs were isolated and digested in 3mg/mL collagenase-dispase mixture for 4 hr. Digested tissues were strained and recovered murine lung endothelial cells (MLECs) were plated on fibronectin coated flasks in DMEM supplemented with 10% FBS, 90μg/mL heparin sulfate, and 50ng/mL endothelial cell growth supplement. MLECs were used in subsequent experiments before passage 3.

NIH-PA Author Manuscript

NIH-PA Author Manuscript

NIH-PA Author Manuscript

### Assays for CEP, hydrogen peroxide, nitrotyrosine, and ROS production

Blood was collected through the vena cava into 0.1M EDTA. Plasma was separated from whole blood by centrifugation. Plasma concentrations of CEP were analyzed by ELISA. 96-well plates (Costar) were precoated with CEP-BSA (220 nM) overnight at 4 °C. Samples were pre-incubated with anti-CEP polyclonal antibody at 37 °C for 1 hour. The supernatant of antibody-antigen complex was then added to the 96-well and incubate at room temperature for 1 hour followed by goat-anti rabbit IgG-HRP secondary antibody (Invitrogen). The reaction was stopped by the addition of 2,2;-azino-bis(3–ethylbenzothiazoline-6-suphonic acid) (ABTS) (Invitrogen) and the data were collected at 405 nm with microplate reader. Plasma concentrations of $H_2O_2$ were determined using a Bioxytech $H_2O_2$-560 Quantitative Hydrogen Peroxide Assay kit (Oxis International) according to the manufacturer's protocol. MLECs were lysed with lysis buffer (20mM Tris, 150mM NaCl, 1mM EDTA, 1mM EGTA, 500mM BHT, 2M DPTA, 0.1% Triton X-100, protease and phosphatase inhibitors). Plasma and MLEC lysates were analyzed for nitrotyrosine concentration using an Amsbio NWLSS Nitrotyrosine ELISA kit according to the manufacturer's protocol. Nitrotyrosine concentrations were normalized to the protein concentration for each sample. Protein concentrations were measured using the Coomassie Plus assay (Thermo scientific). MLECs and macrophages were plated ($1\times10^4$ cells). Cells were treated with 12μg/mL oxLDL for 2 hr and assayed using commercially available kits for ROS production (Invitrogen CM-H2DCFDA Oxidative Stress Indicator) and DNA content (Invitrogen CyQuant NF Cell Proliferation Kit) according to the manufacturer's protocols.

### Oxidized LDL survival

Isolated MLECs and macrophages were treated with oxLDL for 24 hr. Samples were stained in 0.2% trypan blue for 2 minutes, washed in saline, and fixed in 10% formalin for 15 min. Trypan blue stained cells were visualized and counted per field using a Leica DMIL microscope.

### Flow Cytometry

MLECs and macrophages ($1\times10^5$ cells) were blocked with whole molecule murine IgG (1:100) for 15 min. Cells were then incubated with rabbit anti-CD36 antibody (1:20, Abcam) for 1 hr, followed by anti-rabbit-Alexa488 secondary antibody (Molecular Probes) for 30 min. Secondary antibody only stained cells were used as a control for non-specific staining. Samples were washed and fluorescence was measured using a BD FACS CantoII running the BD FACS Diva software. FCS files were exported and analyzed with FlowJo software.

### Statistical Analysis

Student's *t* test analysis, one-way ANOVA analysis with Newman-Keuls post-test, or two-way ANOVA with Boferroni post-test were used to determine statistical significance using GraphPad Prism 4.03 software. Kaplan-Meyer survival curves and a logrank test used to determine statistical significance were prepared using GraphPad Prism. * represents $p<0.05$, ** represents $p<0.01$, and *** represents $p<0.005$.

## Supplementary Material

Refer to Web version on PubMed Central for supplementary material.

## Acknowledgments

We thank Jim Lang for assistance with digital photography, Dr. Qingyu Wu for allowing us to use his microscope, and Dr. Young-Woong Kim for providing the hearts from *ApoE*$^{-/-}$ mice on a high-fat diet. Funding: This study

NIH-PA Author Manuscript

NIH-PA Author Manuscript

NIH-PA Author Manuscript

was supported by research funding from NIH grants DK060933 and HL071625 to T.V.B, HL103952 to P.R.S, and HL077213 to E.A.P. B.A.K was supported by a Ruth L. Kirschstein NRSA award (CA142133) from the NIH/NCI. N.L.M. was supported by an AHA grant (10SDG4300062). Author contributions: B.A.K., L.M., X.Z.W., L.D., N.L.M., M.E.W., A.G., M.T., P.R.S., and M.S.P. performed experiments; B.A.K., L.M., X.Z.W., L.D., and T.V.B. analyzed data; B.A.K., L.M., and T.V.B. designed experiments; B.A.K., E.A.P., and T.V.B. wrote the paper.

## References and Notes

1. Harrison DE, Strong R, Sharp ZD, Nelson JF, Astle CM, Flurkey K, Nadon NL, Wilkinson JE, Frenkel K, Carter CS, Pahor M, Javors MA, Fernandez E, Miller RA. Rapamycin fed late in life extends lifespan in genetically heterogeneous mice. Nature. 2009; 460:392–395. [PubMed: 19587680]
2. Sarbassov DD, Ali SM, Sengupta S, Sheen JH, Hsu PP, Bagley AF, Markhard AL, Sabatini DM. Prolonged rapamycin treatment inhibits mTORC2 assembly and Akt/PKB. Mol Cell. 2006; 22:159–168. [PubMed: 16603397]
3. Lloyd-Jones D, Adams R, Carnethon M, De Simone G, Ferguson TB, Flegal K, Ford E, Furie K, Go A, Greenlund K, Haase N, Hailpern S, Ho M, Howard V, Kissela B, Kittner S, Lackland D, Lisabeth L, Marelli A, McDermott M, Meigs J, Mozaffarian D, Nichol G, O'Donnell C, Roger V, Rosamond W, Sacco R, Sorlie P, Stafford R, Steinberger J, Thom T, Wasserthiel-Smoller S, Wong N, Wylie-Rosett J, Hong Y. Heart disease and stroke statistics--2009 update: a report from the American Heart Association Statistics Committee and Stroke Statistics Subcommittee. Circulation. 2009; 119:480–486. [PubMed: 19171871]
4. Ross R. Atherosclerosis--an inflammatory disease. N Engl J Med. 1999; 340:115–126. [PubMed: 9887164]
5. Trigatti BL, Krieger M, Rigotti A. Influence of the HDL receptor SR-BI on lipoprotein metabolism and atherosclerosis. Arterioscler Thromb Vasc Biol. 2003; 23:1732–1738. [PubMed: 12920050]
6. Braun A, Trigatti BL, Post MJ, Sato K, Simons M, Edelberg JM, Rosenberg RD, Schrenzel M, Krieger M. Loss of SR-BI expression leads to the early onset of occlusive atherosclerotic coronary artery disease, spontaneous myocardial infarctions, severe cardiac dysfunction, and premature death in apolipoprotein E-deficient mice. Circ Res. 2002; 90:270–276. [PubMed: 11861414]
7. Trigatti B, Rayburn H, Vinals M, Braun A, Miettinen H, Penman M, Hertz M, Schrenzel M, Amigo L, Rigotti A, Krieger M. Influence of the high density lipoprotein receptor SR-BI on reproductive and cardiovascular pathophysiology. Proc Natl Acad Sci U S A. 1999; 96:9322–9327. [PubMed: 10430941]
8. Fernandez-Hernando C, Ackah E, Yu J, Suarez Y, Murata T, Iwakiri Y, Prendergast J, Miao RQ, Birnbaum MJ, Sessa WC. Loss of Akt1 leads to severe atherosclerosis and occlusive coronary artery disease. Cell Metab. 2007; 6:446–457. [PubMed: 18054314]
9. Chen J, Somanath PR, Razorenova O, Chen WS, Hay N, Bornstein P, Byzova TV. Akt1 regulates pathological angiogenesis, vascular maturation and permeability in vivo. Nat Med. 2005; 11:1188–1196. [PubMed: 16227992]
10. Chandrasekar B, Marelli-Berg FM, Tone M, Bysani S, Prabhu SD, Murray DR. Beta-adrenergic stimulation induces interleukin-18 expression via beta2-AR, PI3K, Akt, IKK, and NF-kappaB. Biochem Biophys Res Commun. 2004; 319:304–311. [PubMed: 15178407]
11. Boullier A, Li Y, Quehenberger O, Palinski W, Tabas I, Witztum JL, Miller YI. Minimally oxidized LDL offsets the apoptotic effects of extensively oxidized LDL and free cholesterol in macrophages. Arterioscler Thromb Vasc Biol. 2006; 26:1169–1176. [PubMed: 16484596]
12. DeBosch B, Treskov I, Lupu TS, Weinheimer C, Kovacs A, Courtois M, Muslin AJ. Akt1 is required for physiological cardiac growth. Circulation. 2006; 113:2097–2104. [PubMed: 16636172]
13. Haq S, Choukroun G, Lim H, Tymitz KM, del Monte F, Gwathmey J, Grazette L, Michael A, Hajjar R, Force T, Molkentin JD. Differential activation of signal transduction pathways in human hearts with hypertrophy versus advanced heart failure. Circulation. 2001; 103:670–677. [PubMed: 11156878]
14. Sopko N, Qin Y, Finan A, Dadabayev A, Chigurupati S, Qin J, Penn MS, Gupta S. Significance of thymosin beta4 and implication of PINCH-1-ILK-alpha-parvin (PIP) complex in human dilated cardiomyopathy. PLoS One. 2011; 6:e20184. [PubMed: 21625516]

NIH-PA Author Manuscript

NIH-PA Author Manuscript

NIH-PA Author Manuscript


15. Bjedov I, Toivonen JM, Kerr F, Slack C, Jacobson J, Foley A, Partridge L. Mechanisms of life span extension by rapamycin in the fruit fly Drosophila melanogaster. Cell Metab. 2010; 11:35–46. [PubMed: 20074526]
16. Lawlor MA, Alessi DR. PKB/Akt: a key mediator of cell proliferation, survival and insulin responses? J Cell Sci. 2001; 114:2903–2910. [PubMed: 11686294]
17. Somanath PR, Razorenova OV, Chen J, Byzova TV. Akt1 in endothelial cell and angiogenesis. Cell Cycle. 2006; 5:512–518. [PubMed: 16552185]
18. Araki S, Izumiya Y, Hanatani S, Rokutanda T, Usuku H, Akasaki Y, Takeo T, Nakagata N, Walsh K, Ogawa H. Akt1-mediated skeletal muscle growth attenuates cardiac dysfunction and remodeling after experimental myocardial infarction. Circ Heart Fail. 2012; 5:116–125. [PubMed: 22135402]
19. Shiojima I, Sato K, Izumiya Y, Schiekofer S, Ito M, Liao R, Colucci WS, Walsh K. Disruption of coordinated cardiac hypertrophy and angiogenesis contributes to the transition to heart failure. J Clin Invest. 2005; 115:2108–2118. [PubMed: 16075055]
20. Shimizu I, Minamino T, Toko H, Okada S, Ikeda H, Yasuda N, Tateno K, Moriya J, Yokoyama M, Nojima A, Koh GY, Akazawa H, Shiojima I, Kahn CR, Abel ED, Komuro I. Excessive cardiac insulin signaling exacerbates systolic dysfunction induced by pressure overload in rodents. J Clin Invest. 2010; 120:1506–1514. [PubMed: 20407209]
21. Los M, Maddika S, Erb B, Schulze-Osthoff K. Switching Akt: from survival signaling to deadly response. Bioessays. 2009; 31:492–495. [PubMed: 19319914]
22. Dolado I, Nebreda AR. AKT and oxidative stress team up to kill cancer cells. Cancer Cell. 2008; 14:427–429. [PubMed: 19061832]
23. Tsuchiya K, Tanaka J, Shuiqing Y, Welch CL, DePinho RA, Tabas I, Tall AR, Goldberg IJ, Accili D. FoxOs integrate pleiotropic actions of insulin in vascular endothelium to protect mice from atherosclerosis. Cell Metab. 2012; 15:372–381. [PubMed: 22405072]
24. Miller RA, Harrison DE, Astle CM, Baur JA, Boyd AR, de Cabo R, Fernandez E, Flurkey K, Javors MA, Nelson JF, Orihuela CJ, Pletcher S, Sharp ZD, Sinclair D, Starnes JW, Wilkinson JE, Nadon NL, Strong R. Rapamycin, but not resveratrol or simvastatin, extends life span of genetically heterogeneous mice. J Gerontol A Biol Sci Med Sci. 2011; 66:191–201. [PubMed: 20974732]
25. Nogueira V, Park Y, Chen CC, Xu PZ, Chen ML, Tonic I, Unterman T, Hay N. Akt determines replicative senescence and oxidative or oncogenic premature senescence and sensitizes cells to oxidative apoptosis. Cancer Cell. 2008; 14:458–470. [PubMed: 19061837]
26. O'Neill BT, Abel ED. Akt1 in the cardiovascular system: friend or foe? J Clin Invest. 2005; 115:2059–2064. [PubMed: 16075047]
27. Ulici V, Hoenselaar KD, Agoston H, McErlain DD, Umoh J, Chakrabarti S, Holdsworth DW, Beier F. The role of Akt1 in terminal stages of endochondral bone formation: angiogenesis and ossification. Bone. 2009; 45:1133–1145. [PubMed: 19679212]
28. Somanath PR, Chen J, Byzova TV. Akt1 is necessary for the vascular maturation and angiogenesis during cutaneous wound healing. Angiogenesis. 2008; 11:277–288. [PubMed: 18415691]
29. Somanath PR, Kandel ES, Hay N, Byzova TV. Akt1 signaling regulates integrin activation, matrix recognition, and fibronectin assembly. J Biol Chem. 2007; 282:22964–22976. [PubMed: 17562714]
30. Libby P. Inflammation in atherosclerosis. Nature. 2002; 420:868–874. [PubMed: 12490960]
31. Cybulsky MI, Gimbrone MA Jr. Endothelial expression of a mononuclear leukocyte adhesion molecule during atherogenesis. Science. 1991; 251:788–791. [PubMed: 1990440]
32. Minami T, Abid MR, Zhang J, King G, Kodama T, Aird WC. Thrombin stimulation of vascular adhesion molecule-1 in endothelial cells is mediated by protein kinase C (PKC)-delta-NF-kappa B and PKC-zeta-GATA signaling pathways. J Biol Chem. 2003; 278:6976–6984. [PubMed: 12493764]
33. Dweik RA. Nitric oxide, hypoxia, and superoxide: the good, the bad, and the ugly! Thorax. 2005; 60:265–267. [PubMed: 15790976]

NIH-PA Author Manuscript

NIH-PA Author Manuscript

NIH-PA Author Manuscript


34. West XZ, Malinin NL, Merkulova AA, Tischenko M, Kerr BA, Borden EC, Podrez EA, Salomon RG, Byzova TV. Oxidative stress induces angiogenesis by activating TLR2 with novel endogenous ligands. Nature. 2010; 467:972–976. [PubMed: 20927103]
35. Karin M. The NF-kappa B activation pathway: its regulation and role in inflammation and cell survival. Cancer J Sci Am. 1998; 4(Suppl 1):S92–S99. [PubMed: 9619277]
36. Romashkova JA, Makarov SS. NF-kappaB is a target of AKT in anti-apoptotic PDGF signalling. Nature. 1999; 401:86–90. [PubMed: 10485711]
37. Podrez EA, Poliakov E, Shen Z, Zhang R, Deng Y, Sun M, Finton PJ, Shan L, Febbraio M, Hajjar DP, Silverstein RL, Hoff HF, Salomon RG, Hazen SL. A novel family of atherogenic oxidized phospholipids promotes macrophage foam cell formation via the scavenger receptor CD36 and is enriched in atherosclerotic lesions. J Biol Chem. 2002; 277:38517–38523. [PubMed: 12145296]
38. Kar NS, Ashraf MZ, Valiyaveettil M, Podrez EA. Mapping and characterization of the binding site for specific oxidized phospholipids and oxidized low density lipoprotein of scavenger receptor CD36. J Biol Chem. 2008; 283:8765–8771. [PubMed: 18245080]
39. Abel ED, Doenst T. Mitochondrial adaptations to physiological vs. pathological cardiac hypertrophy. Cardiovasc Res. 2011; 90:234–242. [PubMed: 21257612]
40. Li XA, Titlow WB, Jackson BA, Giltiay N, Nikolova-Karakashian M, Uittenbogaard A, Smart EJ. High density lipoprotein binding to scavenger receptor, Class B, type I activates endothelial nitric-oxide synthase in a ceramide-dependent manner. J Biol Chem. 2002; 277:11058–11063. [PubMed: 11792700]
41. Spiecker M, Peng HB, Liao JK. Inhibition of endothelial vascular cell adhesion molecule-1 expression by nitric oxide involves the induction and nuclear translocation of IkappaBalpha. J Biol Chem. 1997; 272:30969–30974. [PubMed: 9388244]
42. Minhajuddin M, Bijli KM, Fazal F, Sassano A, Nakayama KI, Hay N, Platanias LC, Rahman A. Protein kinase C-delta and phosphatidylinositol 3-kinase/Akt activate mammalian target of rapamycin to modulate NF-kappaB activation and intercellular adhesion molecule-1 (ICAM-1) expression in endothelial cells. J Biol Chem. 2009; 284:4052–4061. [PubMed: 19074768]
43. Chen J, De S, Damron DS, Chen WS, Hay N, Byzova TV. Impaired platelet responses to thrombin and collagen in AKT-1-deficient mice. Blood. 2004; 104:1703–1710. [PubMed: 15105289]
44. Yin H, Stojanovic A, Hay N, Du X. The role of Akt in the signaling pathway of the glycoprotein Ib-IX induced platelet activation. Blood. 2008; 111:658–665. [PubMed: 17914025]
45. Condorelli G, Drusco A, Stassi G, Bellacosa A, Roncarati R, Iaccarino G, Russo MA, Gu Y, Dalton N, Chung C, Latronico MV, Napoli C, Sadoshima J, Croce CM, Ross J Jr. Akt induces enhanced myocardial contractility and cell size in vivo in transgenic mice. Proc Natl Acad Sci U S A. 2002; 99:12333–12338. [PubMed: 12237475]
46. Shioi T, McMullen JR, Kang PM, Douglas PS, Obata T, Franke TF, Cantley LC, Izumo S. Akt/protein kinase B promotes organ growth in transgenic mice. Mol Cell Biol. 2002; 22:2799–2809. [PubMed: 11909972]
47. Kops GJ, Dansen TB, Polderman PE, Saarloos I, Wirtz KW, Coffer PJ, Huang TT, Bos JL, Medema RH, Burgering BM. Forkhead transcription factor FOXO3a protects quiescent cells from oxidative stress. Nature. 2002; 419:316–321. [PubMed: 12239572]
48. Nemoto S, Finkel T. Redox regulation of forkhead proteins through a p66shc-dependent signaling pathway. Science. 2002; 295:2450–2452. [PubMed: 11884717]
49. Li XN, Song J, Zhang L, LeMaire SA, Hou X, Zhang C, Coselli JS, Chen L, Wang XL, Zhang Y, Shen YH. Activation of the AMPK-FOXO3 pathway reduces fatty acid-induced increase in intracellular reactive oxygen species by upregulating thioredoxin. Diabetes. 2009; 58:2246–2257. [PubMed: 19592618]
50. Marinkovic D, Zhang X, Yalcin S, Luciano JP, Brugnara C, Huber T, Ghaffari S. Foxo3 is required for the regulation of oxidative stress in erythropoiesis. J Clin Invest. 2007; 117:2133–2144. [PubMed: 17671650]
51. Tothova Z, Kollipara R, Huntly BJ, Lee BH, Castrillon DH, Cullen DE, McDowell EP, Lazo-Kallanian S, Williams IR, Sears C, Armstrong SA, Passegue E, DePinho RA, Gilliland DG. FoxOs are critical mediators of hematopoietic stem cell resistance to physiologic oxidative stress. Cell. 2007; 128:325–339. [PubMed: 17254970]

NIH-PA Author Manuscript

NIH-PA Author Manuscript

NIH-PA Author Manuscript


52. Febbraio M, Podrez EA, Smith JD, Hajjar DP, Hazen SL, Hoff HF, Sharma K, Silverstein RL. Targeted disruption of the class B scavenger receptor CD36 protects against atherosclerotic lesion development in mice. J Clin Invest. 2000; 105:1049–1056. [PubMed: 10772649]
53. Janabi M, Yamashita S, Hirano K, Sakai N, Hiraoka H, Matsumoto K, Zhang Z, Nozaki S, Matsuzawa Y. Oxidized LDL-induced NF-kappa B activation and subsequent expression of proinflammatory genes are defective in monocyte-derived macrophages from CD36-deficient patients. Arterioscler Thromb Vasc Biol. 2000; 20:1953–1960. [PubMed: 10938017]
54. Antonov AS, Kolodgie FD, Munn DH, Gerrity RG. Regulation of macrophage foam cell formation by alphaVbeta3 integrin: potential role in human atherosclerosis. Am J Pathol. 2004; 165:247–258. [PubMed: 15215180]
55. Ming Cao W, Murao K, Imachi H, Sato M, Nakano T, Kodama T, Sasaguri Y, Wong NC, Takahara J, Ishida T. Phosphatidylinositol 3-OH kinase-Akt/protein kinase B pathway mediates Gas6 induction of scavenger receptor a in immortalized human vascular smooth muscle cell line. Arterioscler Thromb Vasc Biol. 2001; 21:1592–1597. [PubMed: 11597931]
56. Lee SH, Park DW, Park SC, Park YK, Hong SY, Kim JR, Lee CH, Baek SH. Calcium-independent phospholipase A2beta-Akt signaling is involved in lipopolysaccharide-induced NADPH oxidase 1 expression and foam cell formation. J Immunol. 2009; 183:7497–7504. [PubMed: 19917703]
57. Chung HY, Cesari M, Anton S, Marzetti E, Giovannini S, Seo AY, Carter C, Yu BP, Leeuwenburgh C. Molecular inflammation: underpinnings of aging and age-related diseases. Ageing Res Rev. 2009; 8:18–30. [PubMed: 18692159]
58. Lu M, Wan M, Leavens KF, Chu Q, Monks BR, Fernandez S, Ahima RS, Ueki K, Kahn CR, Birnbaum MJ. Insulin regulates liver metabolism in vivo in the absence of hepatic Akt and Foxo1. . Nat Med. 2012; 18:388–395. [PubMed: 22344295]
59. Singla DK, Lyons GE, Kamp TJ. Transplanted embryonic stem cells following mouse myocardial infarction inhibit apoptosis and cardiac remodeling. Am J Physiol Heart Circ Physiol. 2007; 293:H1308–H1314. [PubMed: 17416601]
60. Agrawal S, Febbraio M, Podrez E, Cathcart MK, Stark GR, Chisolm GM. Signal transducer and activator of transcription 1 is required for optimal foam cell formation and atherosclerotic lesion development. Circulation. 2007; 115:2939–2947. [PubMed: 17533179]
61. Podrez EA, Poliakov E, Shen Z, Zhang R, Deng Y, Sun M, Finton PJ, Shan L, Gugiu B, Fox PL, Hoff HF, Salomon RG, Hazen SL. Identification of a novel family of oxidized phospholipids that serve as ligands for the macrophage scavenger receptor CD36. J Biol Chem. 2002; 277:38503–38516. [PubMed: 12105195]
62. Iiyama K, Hajra L, Iiyama M, Li H, DiChiara M, Medoff BD, Cybulsky MI. Patterns of vascular cell adhesion molecule-1 and intercellular adhesion molecule-1 expression in rabbit and mouse atherosclerotic lesions and at sites predisposed to lesion formation. Circ Res. 1999; 85:199–207. [PubMed: 10417402]
63. Miller FJ Jr, Gutterman DD, Rios CD, Heistad DD, Davidson BL. Superoxide production in vascular smooth muscle contributes to oxidative stress and impaired relaxation in atherosclerosis. Circ Res. 1998; 82:1298–1305. [PubMed: 9648726]
64. Crabb JW, Miyagi M, Gu X, Shadrach K, West KA, Sakaguchi H, Kamei M, Hasan A, Yan L, Rayborn ME, Salomon RG, Hollyfield JG. Drusen proteome analysis: an approach to the etiology of age-related macular degeneration. Proc Natl Acad Sci U S A. 2002; 99:14682–14687. [PubMed: 12391305]
65. Cai ZP, Shen Z, Van Kaer L, Becker LC. Ischemic preconditioning-induced cardioprotection is lost in mice with immunoproteasome subunit low molecular mass polypeptide-2 deficiency. FASEB J. 2008; 22:4248–4257. [PubMed: 18728217]

NIH-PA Author Manuscript
NIH-PA Author Manuscript
NIH-PA Author Manuscript



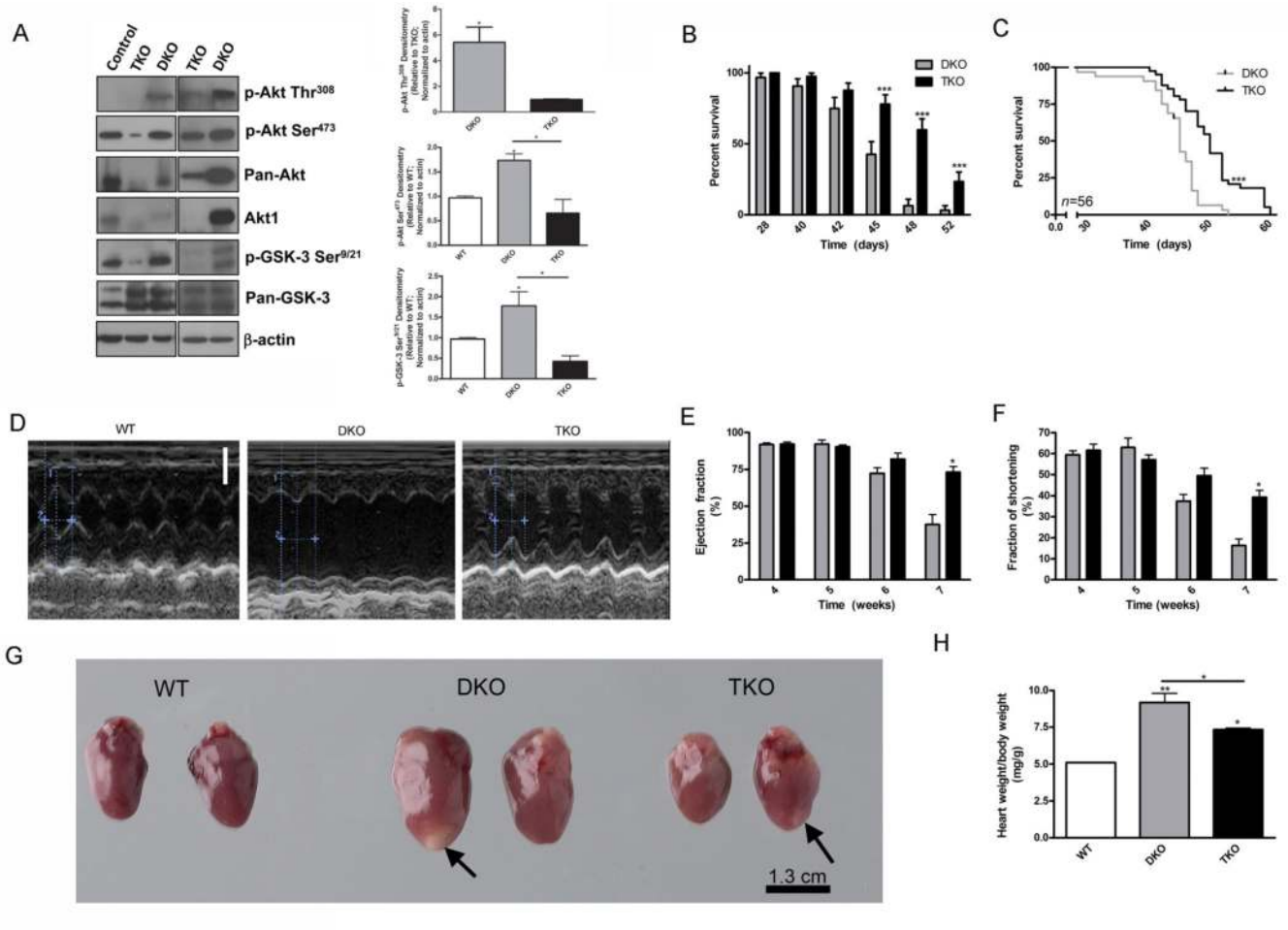


**Fig. 1.**

Akt1 deficiency is associated with extended lifespan, improved cardiac function, and decreased cardiac hypertrophy. **(A)**, Representative immunoblot of phosphorylated (p-) Akt at $Thr^{308}$ (p-Akt $Thr^{308}$), p-Akt at $Ser^{473}$ (p-Akt $Ser^{473}$), pan-Akt, p-GSK-3α/β at $Ser^{9}$ and $Ser^{21}$ (p-GSK-3 $Ser^{9/21}$), pan-GSK-3α/β, and β -actin protein abundance in heart lysates. Densitometry of p-Akt $Thr^{308}$ (top), p-Akt $Ser^{473}$ (middle), and p-GSK-3 $Ser^{9/21}$ (bottom) in heart lysates presented as mean fold change±SEM from TKO mice (top) or wild-type mice (middle and bottom) normalized to actin. (*n*=3–4 mice). **(B)**, Percent survival of mice presented as mean±SEM (*n*=56 mice). **(C)**, Kaplan-Meyer curve depicting the percent survival (*n*=56 mice). **(D)**, Representative echocardiography from wild-type, DKO, and TKO mice. Scale bar represents 0.2 cm. **(E)**, **(F)**, Ejection fraction and fraction of shortening calculated from DKO and TKO heart echocardiography presented as mean percentage±SEM (*n*=11 mice). **(G)**, Representative hearts from mice sacrificed at 42 days of age. Arrows indicate sites of previous infarctions. **(H)**, Ratio of heart weight to body weight presented as mean±SEM (*n*=3 mice). * represents p<0.05, ** represents p<0.01, and *** represents p<0.005 by Student's *t* test compared to DKO (A, C, E, and F), by logrank test compared to DKO (D), or by one-way ANOVA with Newman-Keuls post-test (A and H).

NIH-PA Author Manuscript

NIH-PA Author Manuscript

NIH-PA Author Manuscript

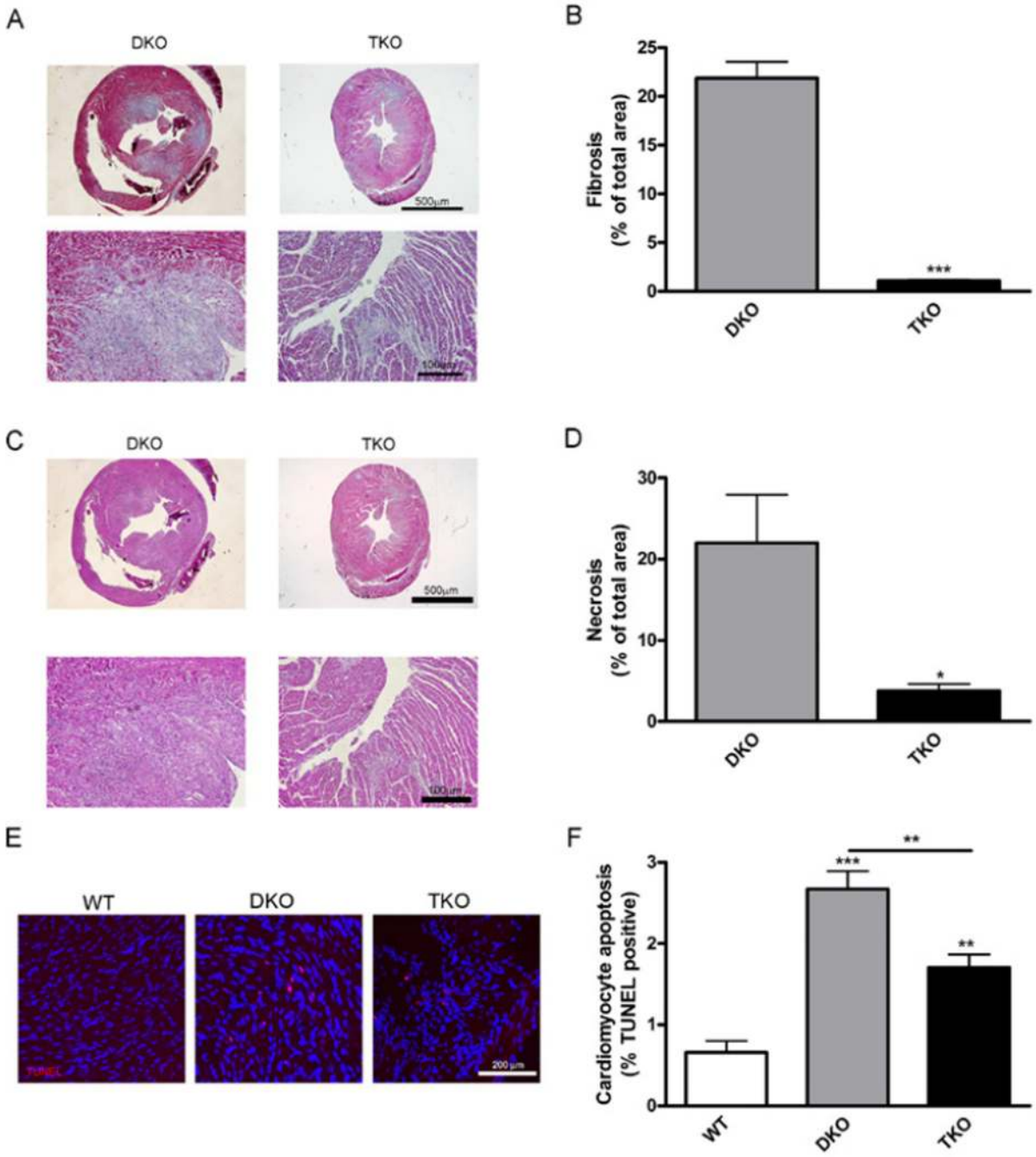


**Fig. 2.**

Akt1 deficiency is associated with decreased development of cardiac fibrosis and necrosis. **(A)**, Representative micrographs of trichrome stained heart serial sections from mice at 42 days of age. **(B)**, Percentage of fibrotic area was calculated using the blue stained collagen and presented as mean±SEM (*n*=5 hearts). **(C)**, Representative micrographs of H&E stained heart serial sections from 42-day-old mice. **(D)**, Percentage of necrotic area calculated from H&E stained sections and presented as mean±SEM (*n*=6 hearts). **(E)**, Representative micrographs of apoptotic cells in hearts stained with TUNEL (red) and DAPI (blue) from 42-day-old mice. **(F)**, Cardiomyocyte apoptosis presented as percent of TUNEL positive

cells±SEM (*n*=3 hearts). * represents p<0.05, ** represents p<0.01, and *** represents p<0.005 by Student's *t* test compared to DKO (B and D) or one-way ANOVA with Newman-Keuls post-test (F).

NIH-PA Author Manuscript
NIH-PA Author Manuscript
NIH-PA Author Manuscript

NIH-PA Author Manuscript

NIH-PA Author Manuscript

NIH-PA Author Manuscript

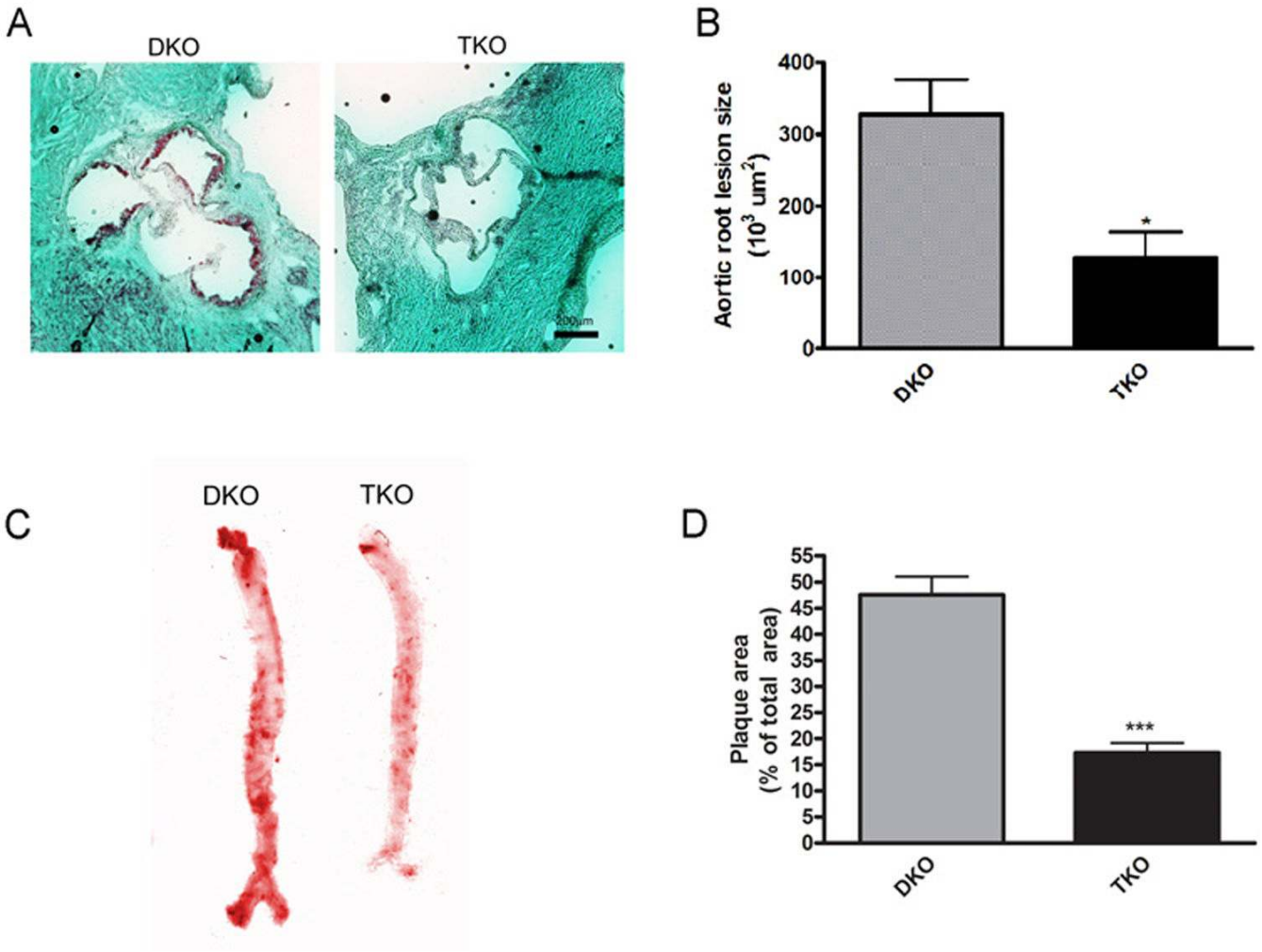


**Fig. 3.**

Loss of Akt1 attenuates spontaneous atherosclerosis. **(A)**, Representative micrographs of Oil Red O stained aortic roots from mice at 42 days of age. **(B)**, Aortic root lesion size presented as mean±SEM (*n*=4 mice). **(C)**, Representative scans of Oil Red O stained aorta from mice at 42 days of age. **(D)**, Plaque area presented as mean percent area±SEM (*n*=4 mice). * represents p<0.05 and *** represents p<0.005 by Student's *t* test compared to DKO.

NIH-PA Author Manuscript
NIH-PA Author Manuscript
NIH-PA Author Manuscript



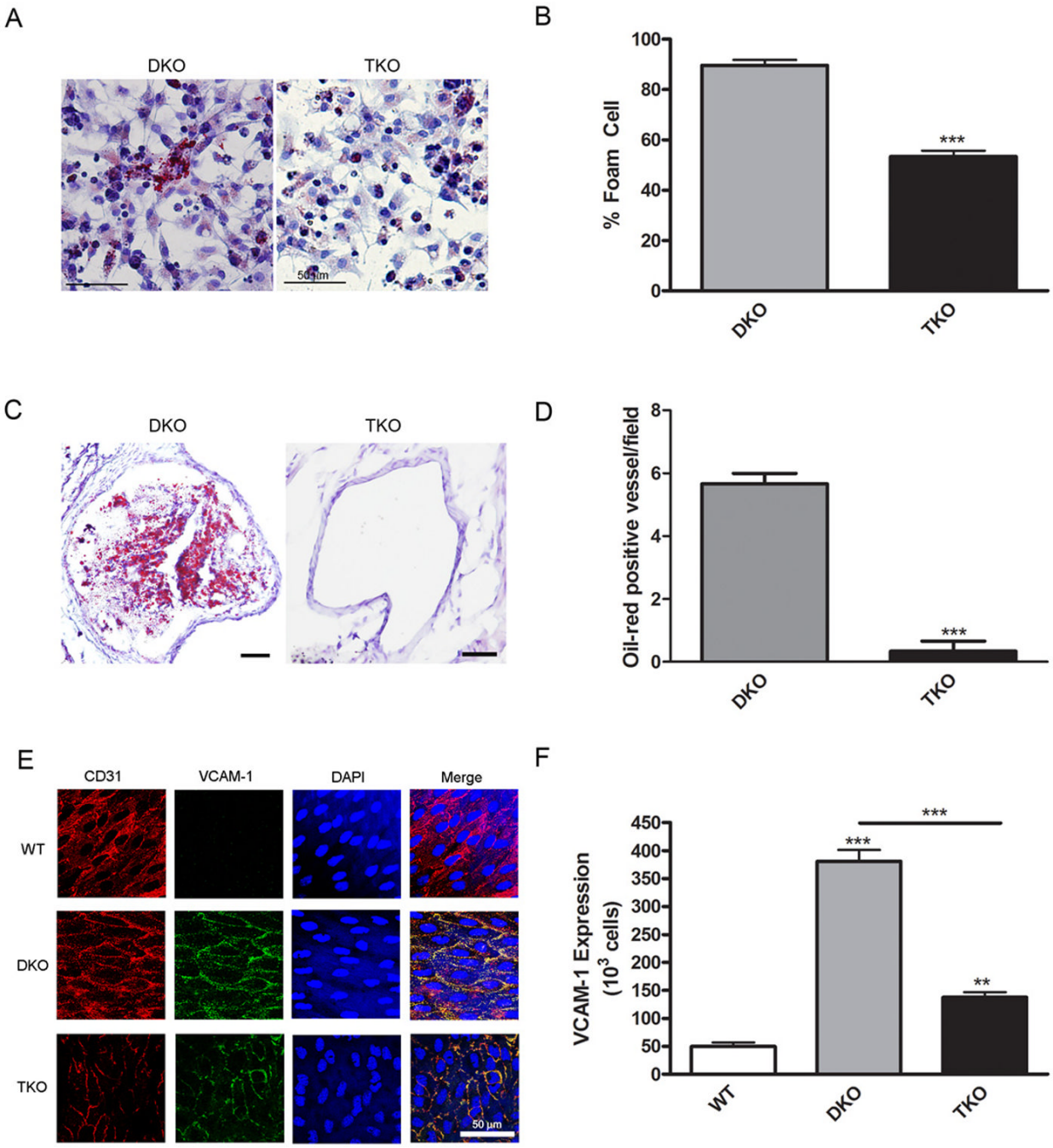


**Fig. 4.**

Akt1 deletion is associated with improved oxidative stress responses. **(A)**, Representative micrographs of Oil Red O stained peritoneal macrophages. **(B)**, Percentage of foam cells per field was calculated and presented as mean±SEM (*n*=9 wells). **(C)**, Representative micrographs of Oil Red O stained coronary arteries. **(D)**, Numbers of stained vessels per field presented as mean±SEM (*n*=4 hearts). **(E)**, Representative micrographs of *en face* aortic sections stained for endothelial cells (CD31, red), VCAM-1 (green) and DAPI (blue). **(F)**, The number of VCAM-1 positive cells were counted and presented as mean±SEM (*n*=3

mice). ** represents p<0.01, and *** represents p<0.005 by Student's *t* test compared to DKO (B and D) or one-way ANOVA with Newman-Keuls post-test (F).

NIH-PA Author Manuscript
NIH-PA Author Manuscript
NIH-PA Author Manuscript

NIH-PA Author Manuscript

NIH-PA Author Manuscript

NIH-PA Author Manuscript

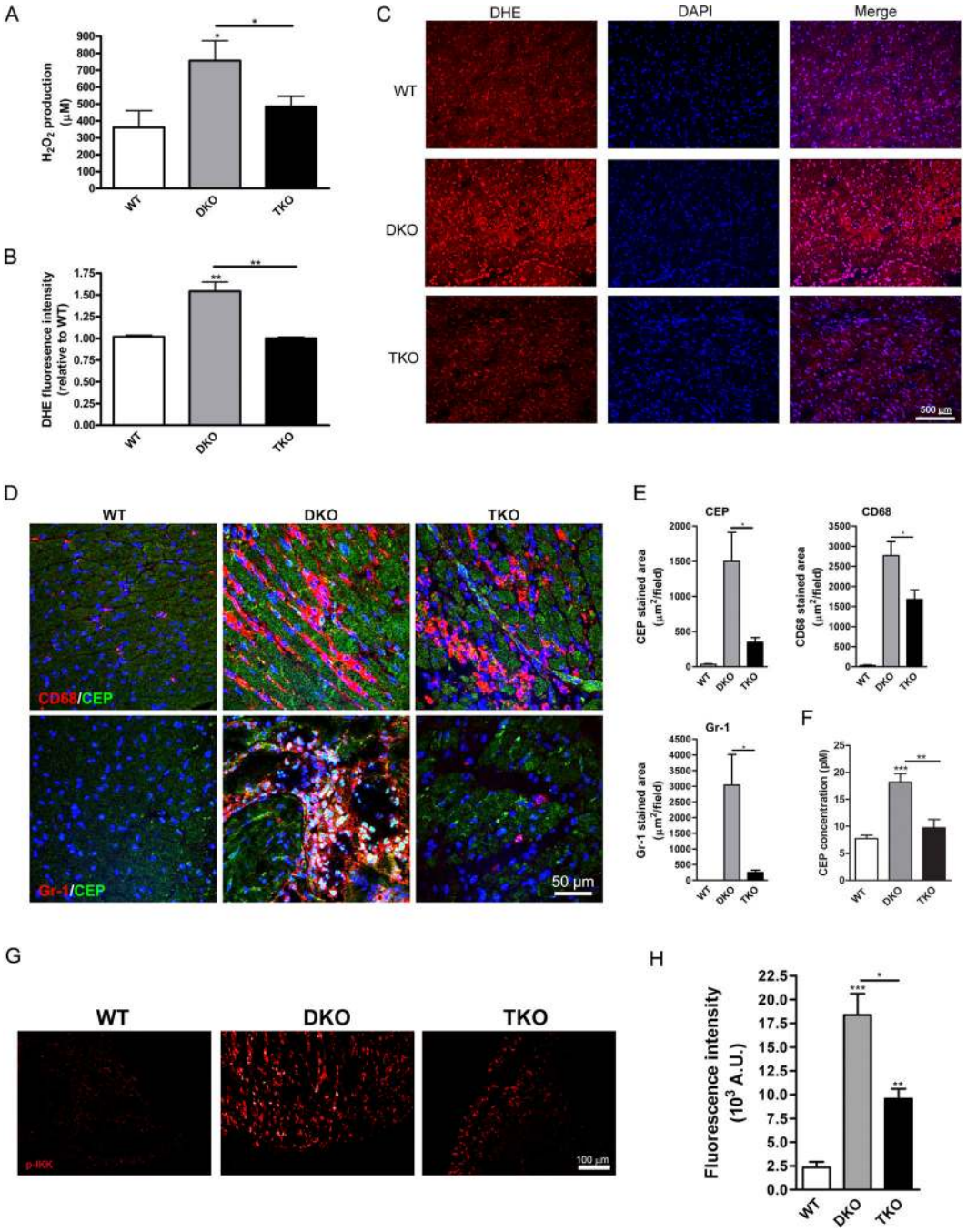


**Fig. 5.**

Akt1 deficiency is associated with decreased ROS generation and inflammation. **(A)**, Hydrogen peroxide was measured in plasma and presented as mean±SEM (*n*=3–6 mice). **(B)**, DHE fluorescence intensity was measured and presented as mean±SEM (*n*=3 hearts). **(C)**, Representative micrographs of heart sections stained for superoxide production (DHE, red) and DAPI (blue). **(D)**, Representative micrographs of heart sections stained for oxidation products (CEP, green) and either macrophages (CD68, red, top panels) or neutrophils (Gr-1, red, bottom panels). **(E)**, Stained area was calculated for CEP (top left), CD68 (top right) and Gr-1 (bottom left) and presented as mean±SEM (*n*=5 hearts). **(F)**,

NIH-PA Author Manuscript

NIH-PA Author Manuscript

NIH-PA Author Manuscript

Plasma concentrations of CEP presented as mean±SEM (*n*=4 mice). **(G)**, Representative micrographs of heart sections stained for phosphorylated IKKα/β (p-IKK, red) as an indicator of NF-κB signaling. **(H)**, Fluorescence intensity of p-IKK staining was quantified and presented as mean±SEM (*n*=3 hearts). * represents $p<0.05$, ** represents $p<0.01$, and *** represents $p<0.005$ by one-way ANOVA with Newman-Keuls post-test.

NIH-PA Author Manuscript
NIH-PA Author Manuscript
NIH-PA Author Manuscript



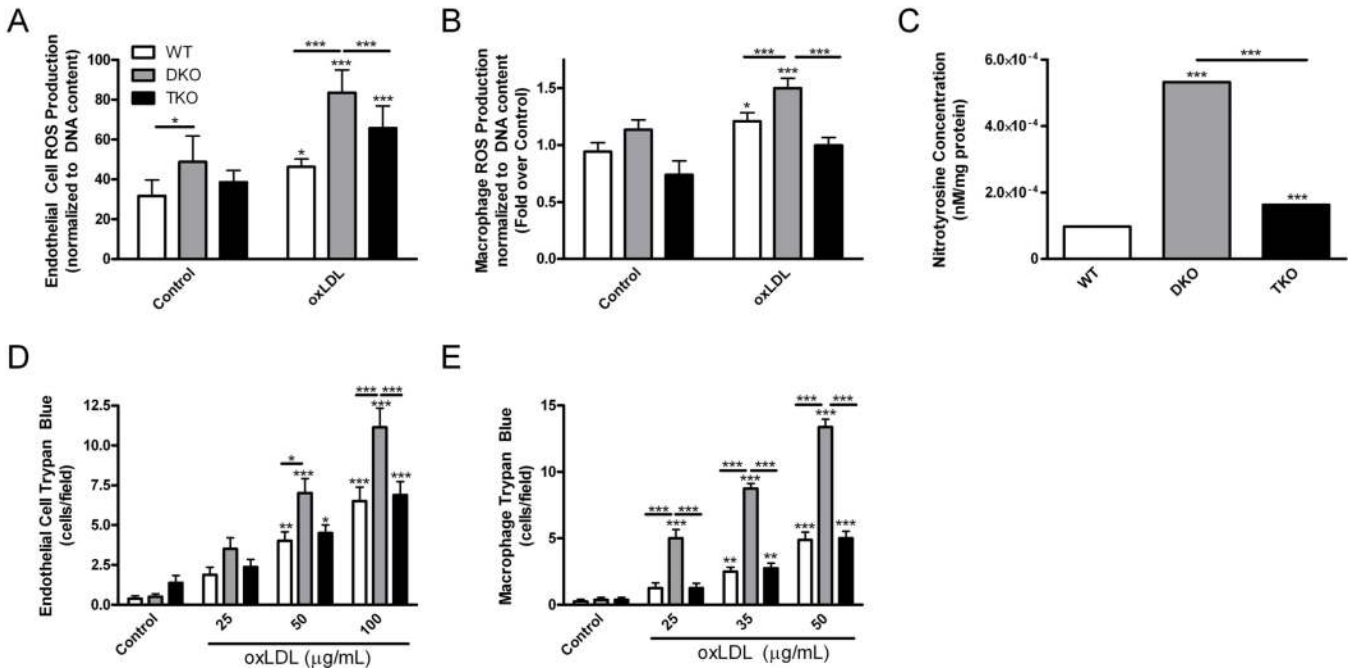


**Fig. 6.**

Loss of Akt1 is associated with decreased ROS production and improved survival after ROS challenge in endothelial cells and macrophages. **(A), (B)**, ROS production in MLEC and peritoneal macrophages treated with oxidized LDL (oxLDL) presented as mean±SEM normalized by DNA content (*n*=8 wells). **C**, Nitrotyrosine concentration in MLEC presented as mean±SEM (*n*=3 mice). **(D), (E)**, Survival of MLECs and peritoneal macrophages treated overnight with oxLDL, presented as mean trypan blue stained cells per field±SEM (*n*=8 wells). * represents p<0.05, ** represents p<0.01, and *** represents p<0.005 by two-way (A, B, D and E) with Bonferroni post-test or one-way ANOVA with Newman-Keuls post-test (C).

NIH-PA Author Manuscript

NIH-PA Author Manuscript

NIH-PA Author Manuscript

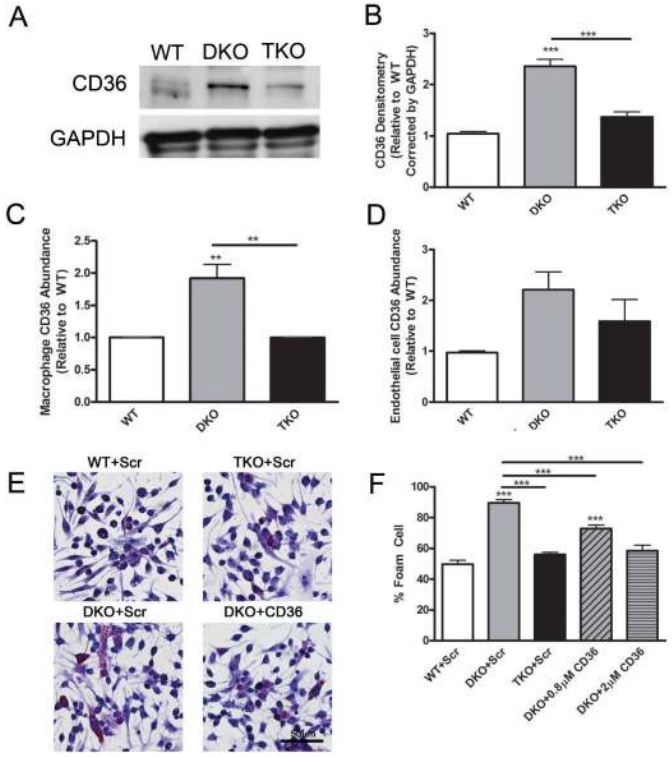


**Fig. 7.**

Alterations in CD36 abundance occur in response to Akt1 activation and can partially rescue Akt1 induced atherosclerosis. **(A)**, Representative immunoblot of CD36 and GAPDH abundance in heart lysates. **(B)**, Densitometry of CD36 abundance in heart lysates presented as fold change over wild-type corrected by GAPDH (*n*=3 mice). **(C), (D)**, CD36 surface abundance on macrophages and MLECs presented as mean fold change over wild-type ±SEM (*n*=4 mice) measured by flow cytometry. **(E)**, Macrophages were treated with scrambled peptides (Scr) or CD36 blocking peptides (CD36) in combination with oxLDL and stained with Oil Red O. **(F)**, Percentage of foam cells per field was calculated and presented as mean±SEM (*n*=9 wells). ** represents p<0.01 and *** represents p<0.005 by one-way ANOVA with Newman-Keuls post-test.

NIH-PA Author Manuscript

NIH-PA Author Manuscript

NIH-PA Author Manuscript

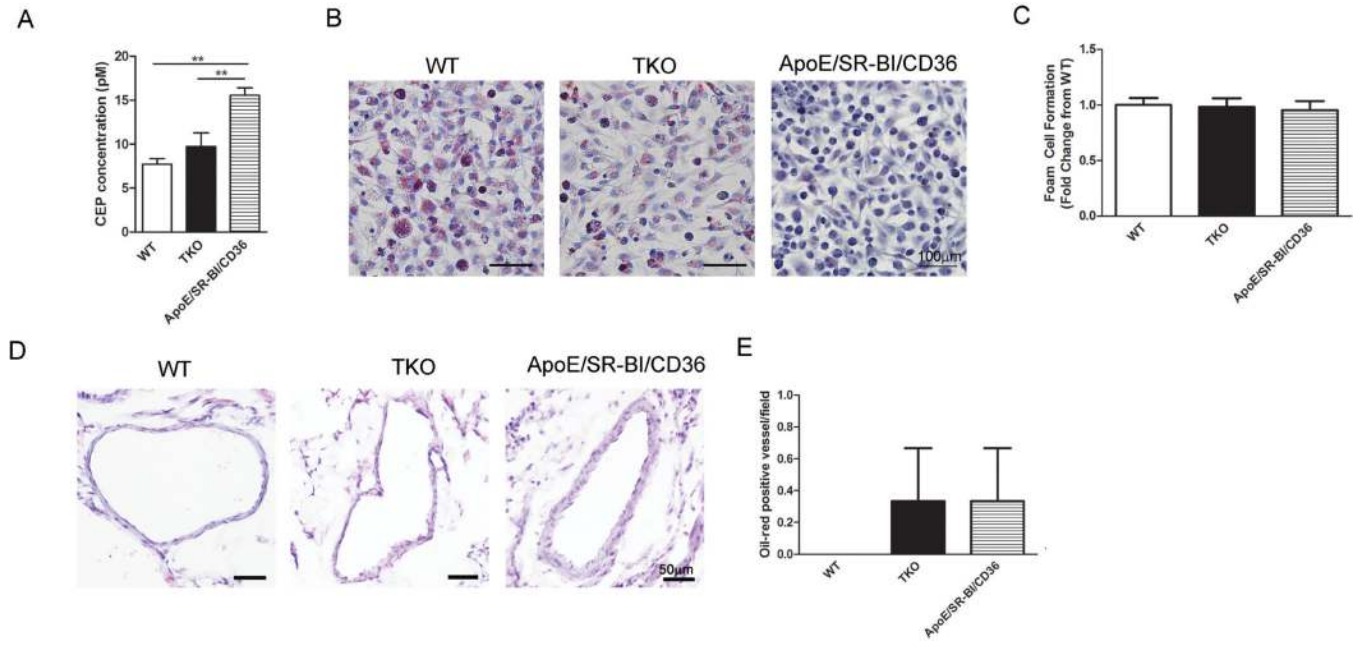


**Fig 8.**

CD36 deletion on the DKO background reduces atherosclerosis, but not oxidative stress. **(A)**, Plasma concentrations of CEP represented as mean±SEM (*n*=4 mice). **(B)**, Macrophages were treated with oxLDL and stained with Oil Red O. **(C)**, Percentage of foam cells per field presented as mean fold change from wild-type±SEM (*n*=9–10 wells). **(D)**, Representative micrographs of Oil Red O stained coronary arteries. **(E)**, Numbers of stained vessels per field presented as mean±SEM (*n*=4 hearts). ** represents p<0.01 by one-way ANOVA with Newman-Keuls post-test.